ADVANCED PHOTONICS RESEARCH
Open Access
www.adpr-journal.com

Extraordinarily Transparent Metaldielectrics for Infrared and Terahertz Applications

Xiaofei Xiao, Mariacristina Turino, I. Brian Becerril-Castro, Stefan A. Maier, Ramon A. Alvarez-Puebla, and Vincenzo Giannini**

Metamaterials are extremely important in advanced technologies, but usually, they rely on the resonant behavior of their constituent blocks. This strongly limits the application of metamaterials to particular frequency band ranges. However, metamaterials with broadband behaviors are highly desirable and are essential for many applications. Herein, recently discovered metamaterials that are composed of densely packed metallic nanoparticles but behave as effective dielectrics are explored. Such metamaterials are extremely transparent for all wavelengths within or exceeding the near infrared and their performance is constant across an ultra-broadband range of frequencies, which is vital to many devices that operate across the same frequency range. The ability to tune the refractive index of these metamaterials to unnaturally high values while maintaining transparency opens new avenues, such as creating flat, thin metalenses in the terahertz region where only bulk lenses are currently available. To highlight those features, several new possible infrared and terahertz applications of these metamaterials which push the boundary of existing technology in THz photonics are shown.

1. Introduction

The development of technology has historically shown a strong link to the capabilities of available materials. Metamaterials have shown promise in advancing technology by enabling novel behaviors that are derived not directly from their constituent materials, but from their subwavelength structures[1,2] and, even more recently, active control.[3] In optics, metamaterials have delivered groundbreaking applications in electromagnetism and photonics,[4–6] such as focusing and imaging with subwavelength resolution[7] and negative refraction,[8] and have thus attracted great interest during the last decades. These subwavelength structures are able to directly tailor light properties including amplitude, phase, and polarization.

Owing to their ability to support surface plasmon polaritons,[9] noble metals such as silver and gold have been the traditional material choice for building blocks in visible metamaterials while plasmonic terahertz (THz) nanoantennas are generally based on heavily doped semiconductors.[10] However, these metamaterials usually rely on the resonant behavior of their constituent blocks and there are high resistive losses at optical frequencies, which restrict the functionality of such metamaterials and related devices to sharp frequency band ranges. More generally, metamaterials based on resonant behavior work only around the

X. Xiao, V. Giannini
Advanced Materials Research Center
Technology Innovation Institute
Building B04C, 9639 Masdar City, Abu Dhabi, United Arab Emirates
E-mail: xiaofei.xiao@tii.ae; vincenzo.giannini@csic.es

M. Turino, I. B. Becerril-Castro, R. A. Alvarez-Puebla
Department of Physical Chemistry and EMaS
Universitat Rovira i Virgili
43007 Tarragona, Spain

S. A. Maier
School of Physics and Astronomy
Monash University
Clayton, Victoria 3800, Australia

The ORCID identification number(s) for the author(s) of this article can be found under https://doi.org/10.1002/adpr.202200190.

DOI: 10.1002/adpr.202200190

S. A. Maier
The Blackett Laboratory
Imperial College London
London SW7 2AZ, UK

S. A. Maier
Chair in Hybrid Nanosystems, Nanoinstitute München
Faculty of Physics
Ludwig-Maximilians-Universität München
80539 München, Germany

R. A. Alvarez-Puebla
ICREA
Passeig Lluis Companys 23, 08010 Barcelona, Spain

V. Giannini
Instituto de Estructura de la Materia (IEM-CSIC)
Consejo Superior de Investigaciones Científicas
Serrano 121, 28006 Madrid, Spain

V. Giannini
Centre of Excellence ENSEMBLE3 sp. z o.o.
Wolczynska 133, 01-919 Warsaw, Poland

frequency of their resonances, making them intrinsically narrowband.

On the other hand, the infrared and THz region of the electromagnetic spectrum has been widely used in industrial, scientific, military, and medical applications.[11,12] In particular, the THz frequency band (0.1–10 THz) shows great promise for many vital applications and has attracted considerable attention in a variety of fields including security, molecular recognition, and medical imaging.[13] However, techniques using THz science are still immature compared with the technologies operating in the optical frequency range. Although the commonly used infrared materials include germanium, sapphire, calcium fluoride, and zinc sulfide, one of the main issues in infrared and THz sciences is the lack of thin and versatile optical devices operating in this wavelength range. For these reasons, the pursuit of new dielectric materials capable of manipulating infrared and terahertz waves is attractive. It is moreover highly desirable to have achromatic metamaterials with broadband behaviors, which are useful to many applications.[14–16] Creating a metalens that operates across a broad range of frequencies would require a metamaterial with constant performance across the same frequency range.

In this direction, it has recently been demonstrated that compact metallic metamaterials can provide unnatural high refractive indexes[17,18] and at the same time are extremely transparent for all wavelengths within or beyond the near infrared.[16] Due to their unique properties we will refer to these metamaterials as "*metaldielectrics*" to highlight their effective dielectric character even if made of metallic components.

The "first metamaterial" realized by Kock in 1948[19] was made of centimeter-scale arrays of metallic particles that behave as dielectrics in the microwave frequency region.[19] Such centimeter-scale structures (known as artificial dielectrics) are also transparent, though this is not surprising because at such frequencies metals approximate perfect conductors so that no field can penetrate into the metal and be absorbed. In contrast, metallic nanoparticles used to build metaldielectrics have dimensions comparable or even much smaller than the skin depth, allowing field penetration, and as such incline to high absorption, at least in principle.

Recently, in a series of really interesting works, first theoretically[20,21] and later experimentally,[22,23] it was demonstrated that these metamaterials present positive refractive indices that can be very high. However, the effective refractive index is complex for metallic metamaterials and it tends to have a large, unwanted, imaginary part that prevents field penetration. In other words, if we want the benefit of the highly effective refractive index of these metamaterials, we should minimize its imaginary part. The conditions of transparency were analyzed in the study by Palmer et al.,[16] where it was also demonstrated that usually a simple Maxwell–Garnett formula provides the effective dielectric constant with good accuracy. The experimental works on transparent compact metallic metamaterials just started, but the phenomenon has been already undoubtedly observed.[16,18]

These metamaterials are showing increasing interest in the scientific community, thanks to their possible applications.[17,18,24,25]

In this work, we demonstrate that metaldielectrics provide a promising optical material platform enabling us to design broadband infrared and terahertz devices and systems. We show that metaldielectrics offer a favorable solution for producing effective dielectrics with large index gradients, especially at infrared and terahertz, thanks to their inherently "programmable" properties. Metaldielectrics with more complex optical properties, such as anisotropy, can be created by altering the structural geometry (including the size, shape, and spacing of the nanoparticles, and the lattice) and the constituent materials (of both host and inclusions). The latter is essential in many applications,[26,27] including devices based on the idea of transformation optics.[28] The ability to tune the refractive index of these metamaterials to unnaturally high values[17,18] while maintaining transparency across a broad range of frequencies[16] opens new avenues, such as creating flat, thin metalenses in the THz region where only bulky lenses are currently available. Light interaction with metallic metastructures in the long-wavelength regime shows exciting advances.[29,30] Here, we show several new possible applications of these metamaterials which push the boundary of existing technology in photonics.

2. Results and Discussion

Figure 1a shows the experimental realization of the metaldielectric concept, that is, a macroparticle structure made of many small metal nanoparticles. In a bulk metal (Figure 1b), the atoms are bound together in a way that allows electrons to move through the material more or less freely. When an external electric field is applied, those free electrons are driven to the metal surfaces to generate an internal electric field that cancels the applied field inside. Therefore, bulk metals are highly opaque below the plasma frequency (usually in the frequency range of visible light and below). In striking contrast, metallic nanoparticle arrays can offer very high transparency over ultra-broadband ranges of wavelengths from microms up to millimeters or more exceeding in some cases[16] the transparency of commonly used infrared materials, such as germanium. This is because although metal nanoparticles possess free electrons, these electrons only move freely within the confines of the nanoparticles, as shown in Figure 1c. In this sense, the separated particles can be regarded as the "meta-molecules" or "-atoms", and the metallic nanoparticle array effectively mimics a traditional bulk dielectric. This physical picture also applies to densely packed arrays[16] of metallic nanoparticles with complex geometries, when free electrons are bound to each "meta-atom".

It is worth noting that the transparency is not related to the generation of plasmon bands resulting from the structure periodicity.[32] In fact, specially at visible wavelengths where surface plasmon resonances occur, these metallic arrays, even with a low filling fraction, would present losses.[33] At longer operating wavelengths, the metallic particles within metaldielectrics, despite being smaller than the metal skin depth, show negligible losses such that the arrays are highly transparent.[16]

In order to quantify the effective properties of metamaterials, different homogenization principles, including both analytical methods[34,35] and numerical methods,[36,37] have already been developed. However, so far, it remains very challenging to obtain the relevant material parameters of densely packed arrays of metallic nanoparticles when the components are very lossy,

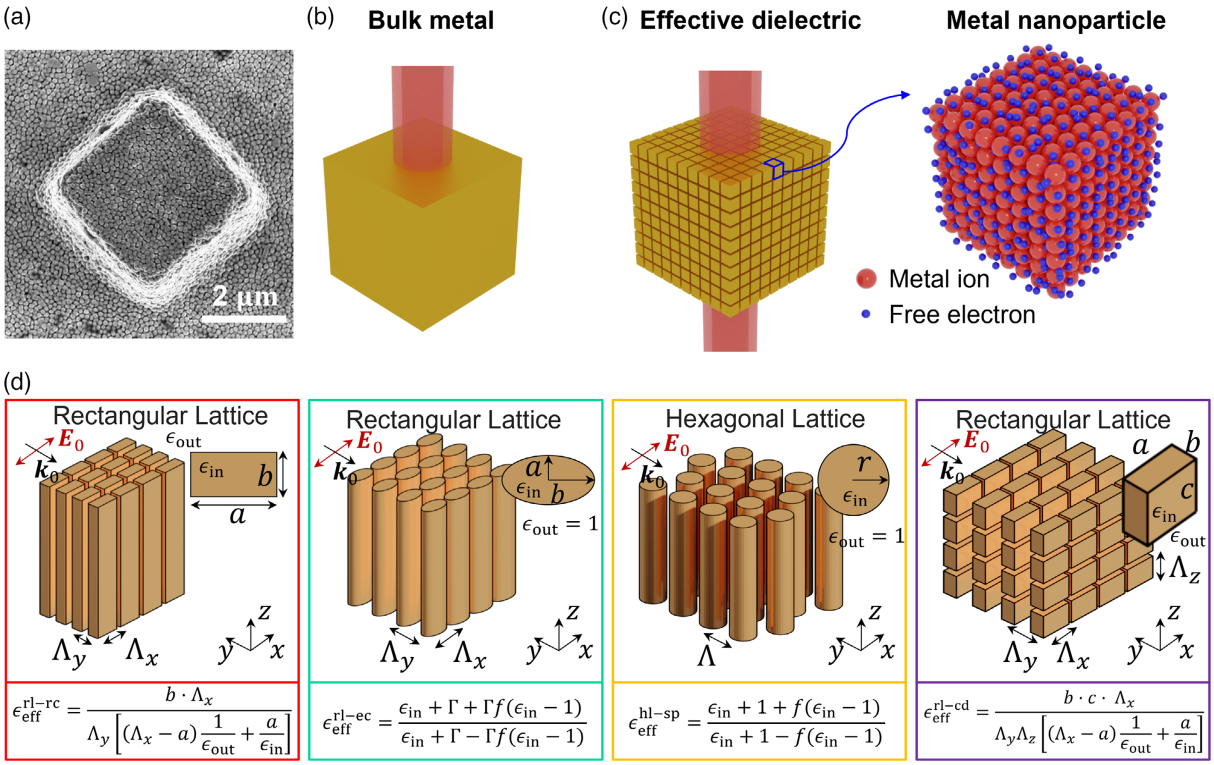

Figure 1. Metaldielectric concept: a) example of a metamaterial (scanning electron microscopy image) composed of dense metal nanoparticles following the study by Tebbe et al.[31] While b) bulk metals are typically highly opaque, c) metaldielectrics can be extraordinarily transparent. Electrons move freely within metallic nanoparticles but they are confined within each metal particle. In this sense, these particles can be considered as analogous to the "molecules" or "atoms" in traditional bulk dielectrics. d) Analytical effective permittivity for four common configurations when light is polarized along x direction and impinges from y direction. In the second and third case, $\Gamma = b/a$ and f denotes the filling fraction of the cylinders.

highly dispersive, and strongly coupled due to the close packing. Anyway, when the wavelength is much bigger than the periodicity and the metal has a large negative real part of the permittivity, some useful analytical formula can be derived, as shown in Figure 1d.

In this work, a numerical effective parameter retrieving method proposed in the study by Palmer et al.[16] is used to extract the effective complex refractive index n_{eff} of the metaldielectrics with high accuracy, by solving an electromagnetic eigenvalue problem and using experimental tabulated data for the metals dielectric constant.[38] Being the magnetic response small for the system and wavelengths considered in this article, the effective permittivity reads $\epsilon_{\text{eff}} = n_{\text{eff}}^2$. Without loss of generality, the geometry considered here for the theoretical proposals is constructed by periodic square arrays of square cylinders, as shown in the insets of **Figure 2**a.

We show in Figure 2 the effective refractive index of nanoparticle arrays for four configurations with different metals (Au and Ti) and/or surrounding refractive indices ($n_s = 1.0$ and 1.5). The calculations are done in the infrared and THz regime (30–300 μm). To investigate the metaldielectrics, we begin by focusing on each individual case. Figure 2 shows that metallic nanocylinder arrays behave as effective dielectrics ($\Re\{\epsilon_{\text{eff}}\} > 0$) for transverse electric (TE)-polarized incidence as expected, due to oscillating surface charges under a transverse force, leading to the oscillating dipoles, which mimic the polarization effect in a real dielectric. It is also shown that such arrays are virtually dispersion free over ultra-broadband ranges of wavelengths from 30 μm up to more, enabling the design of achromatic optical components with ultrabroad bandwidth.

We can observe that the real part of the effective refractive indexes of arrays with different metals, but the same geometry, and surrounding refractive index, are tending to the same value. On the other hand, the imaginary parts of the effective refractive indices in Figure 2a,c (or Figure 2b,d) are different and can be explained by the different skin depths of the two metals. In fact, Figure 2a,c (or Figure 2b,d) suggest that metals with longer skin depths produce the most transparent (least lossy) and least dispersive nanoparticle arrays.[16] The presence of surrounding material filling between the metallic nanoparticles (Figure 2b, d) leads to substantial amplification of the effective refractive index compared with metallic metamaterials in vacuum (Figure 2a,c). In this way, it is possible to achieve an unprecedentedly large effective refractive index by further reducing the gap width and filling the gap with materials with higher refractive indices.[18,23] Metaldielectrics therefore significantly expand the range of available materials with a desirable refractive index.

In addition, the gap width (defined by $g = P - L$, where P and L are the array period and the particle size, respectively) plays a crucial role in tuning the effective refractive index. The effective refractive index (and hence the effective permittivity) shows an asymptotic behavior depending on the gap width. Although the

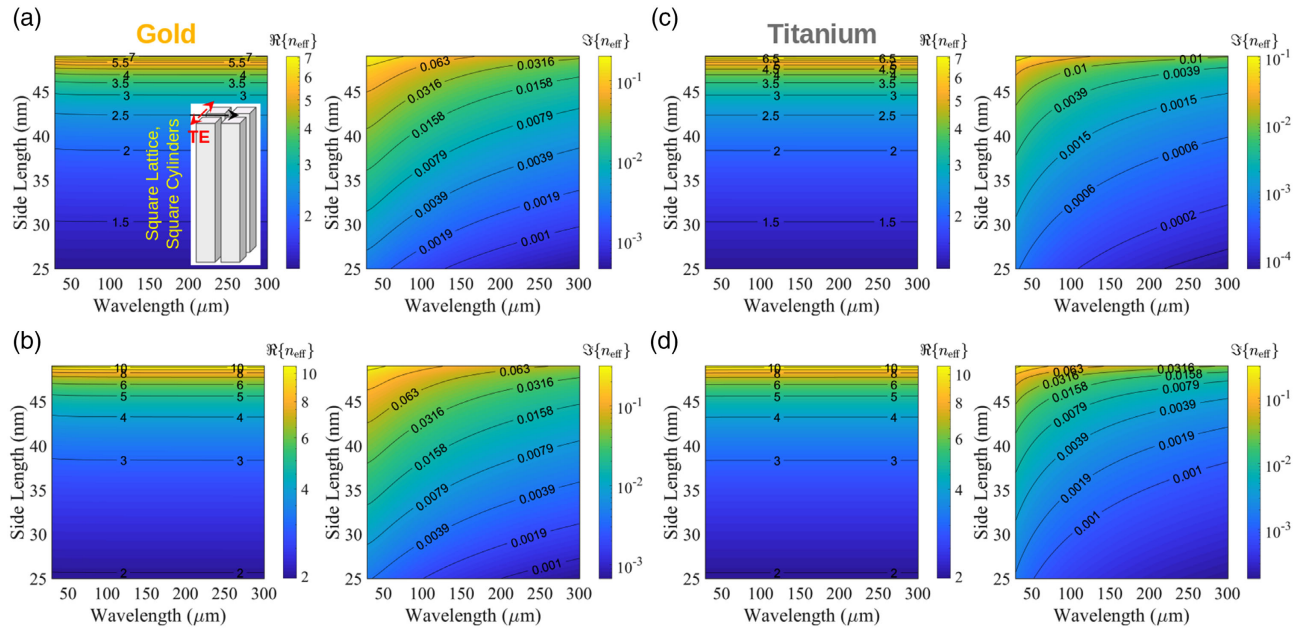

Figure 2. Effective refractive index of metaldielectrics (real part and imaginary part). Arrays are constituted by square nanocylinders arranged in a square lattice with a period of 50 nm (inset). The material of the particles is a,b) gold and c,d) titanium, respectively. The surrounding refractive indices (n_s) are 1 (a,c) and 1.5 (b,d), respectively. In the inset of (a), the red and black arrows denote the electric field and the wave vector of the incident light.

effective refractive index will increase as the gap width decreases, the growth speed differs significantly in weakly coupled ($g/P \approx 1$) and strongly coupled ($g/P \ll 1$) regimes, as the behavior of the charge accumulation differs significantly.[16,39]

Figure 2 shows that the losses remain very low in four cases, enabling the design of optical components that require extraordinarily transparent materials. It is worth noting that in addition to the gap width and the surrounding materials, the structural geometry (including the size, shape of the nanoparticles, and the lattice) and the constituent materials can be altered to tune the effective behaviors of the metaldielectrics, and even provide spatial control on the local refractive indies over a defined volume, which is essential in many applications, such as the ones proposed in transformation optics.

2.1. THz Antireflection Coatings

To test the accuracy of the used method and to validate our effective refractive index calculations, we compare the results calculated using the effective geometry and the full geometry for two types of antireflection (AR) coatings, which are used to enhance the light transmission or absorption efficiency by reducing surface reflections for a target wavelength or a wide wavelength range.

The first one is a single-layer AR coating using the simplest interference concept, requiring a single transparent thin layer of material with refractive index (n_1) equal to the square root of the refractive index of the substrate,[40] as shown in **Figure 3**a. We can use the gold nanocylinders arrays shown in Figure 2a to form this AR coating layer, as shown in the inset of Figure 3a. As the period of the array is set as 50 nm, the layer thickness d is set as 4 μm.

The results of reflection and transmission in three simulations using the effective geometry based on the transfer matrix method (TMM) without (T1 and R1) and with (T2 and R2) considering the dispersion and the full geometry (T3 and R3) based on the finite-difference time-domain (FDTD) method are shown in Figure 3b. As expected, such a coating gives zero reflectance for light with wavelength $\lambda_0 = 4mn_1d$, where m denotes a positive integer. The transmission peaks in Figure 3b indicate that the metallic metamaterials proposed are low loss and extraordinarily transparent at the wavelengths of interest. Results of the effective geometry and the full geometry agree well. The small discrepancies of the results between T1 and T2 are mainly due to the dispersion of gold, while the small discrepancies of the results between T2 and T3 are mainly due to the truncation of the nanocylinder particles. It is finally worth noting that the dispersion of metaldielectrics is very small.

To highlight the tuning possibilities of the local effective index, we construct a THz gradient-index (GRIN) AR coating using the same square lattice of gold nanocylinders that was studied in Figure 2a but varying the dimensions of the cylinders with position and increasing the layer thickness to 50 μm. The schematics of the GRIN AR coating and size-dependent effective refractive index of gold nanocylinders at a wavelength of 30 μm are shown in Figure 3c. Note that, to simplify the simulation and reduce fabrication requirements, the value of particle size (in units of nanometers) is rounded to the nearest integer. Reflection and transmission of this GRIN AR coating calculated using TMM for the effective geometry and the finite-element method (FEM) for the full geometry are illustrated in Figure 3d, indicating that an ultrabroad band GRIN AR coating is realized. It is worth to note that thin AR coatings in the THz region are highly desirable. In order to get a higher transmission

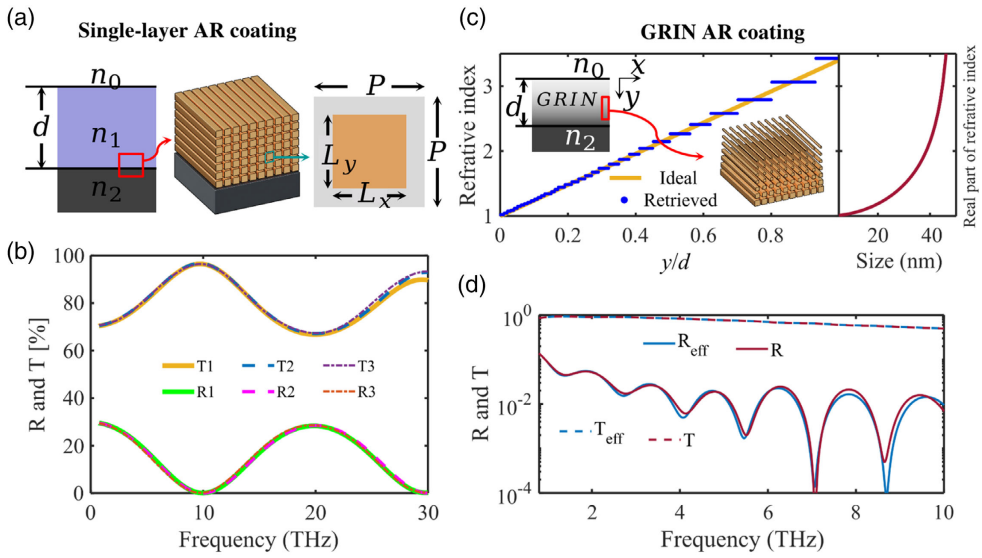

Figure 3. AR coatings. a) Schematics of a single-layer AR coating. b) Its reflection and transmission spectra, when $n_0 = 1$, $n_2 = 3.4$, and $d = 4\,\mu m$. T1 and R1 are calculated using TMM for the effective geometry with fixed $n_1 = \sqrt{n_0 n_2} = 1.844$. T2 and R2 are calculated using TMM method with frequency-dependent effective refractive index retrieved from the following parameters of the unit cell: gold square cylinder, $P = 50\,nm$, $L_x = L_y = 37\,nm$. T3 and R3 are obtained using FDTD method with the same configuration as the one for R2, but for the full geometry. c) Designed and retrieved refractive index for GRIN AR coating, and the relation between the particle (gold) size and real part of the effective refractive index at a wavelength of 30 μm. For simplification, the value of particle size (in units of nanometers) is rounded to the nearest integer. d) Reflection and transmission of the GRIN AR coating, when $n_0 = 1$, $n_2 = 3.4$, $d = 50\,\mu m$. The spectra are calculated using TMM for the effective geometry (labeled with R_{eff} and T_{eff}) and FEM for the full geometry (labeled with R and T), respectively, where we can appreciate broadband transmission.

(i.e., to make the system more transparent), we can use metals, such as titanium, with longer skin depths (Figure S1, Supporting Information) to further suppress the absorption. This suggests that we can easily create devices that operate across a broad range of frequencies using metaldielectrics with constant performance across the same frequency range. In addition, we also prove that the electromagnetic properties of the effective geometries coincide with the ones of the full geometries. The small discrepancies of the results between the effective geometry and the full geometry are mainly due to the dispersion of gold, the truncation of the nanocylinder dimension, and the numerical errors.

In addition to producing ultra-broadband achromatic optical components with 2D nanocylinder arrays, the metaldielectrics composed of 3D nanoparticles allow us to realize the most complex and general optical component designs requiring the ability to spatially manipulate the local refractive indices in 3D, thanks to the inherently programmable properties of metaldielectrics.

From a mathematical perspective, Maxwell's equations are form-invariant under coordinate transformations. In order to convey the effect of the coordinate transformation to the electromagnetic fields, the medium through which light travels needs to transform into an inhomogeneous medium.[1] Based on this idea, transformation optics was proposed and has been used to design devices with novel functionalities.[1] Refractive index profiles play an essential part in transformation optics. However, manufacturing optically inhomogeneous media with large index gradients in a controlled manner poses great challenges. Although some devices in 2D have been experimentally fabricated,[41] real 3D designs are very hard to achieve experimentally. Here we apply the proposed metallic nanoparticle arrays to produce several refractive index profiles achieving images with almost no aberration in 3D, which can operate over a broad range of frequencies due to the extremely small dispersion of the effective refractive index. Schematics of a GRIN lens composed of metal nanoparticles with different sizes are shown in **Figure 4**a.

2.2. GRIN Lenses

We now consider the refractive index profiles of the three most common lens designs, namely, a Luneburg lens, a Maxwell's fish-eye lens, and a light concentrator, as shown in Figure 4b,d,f. Due to the high complexity and fine details required for simulations using the full geometries, effective geometries were used in the FEM simulations. The corresponding near-field distributions are shown in Figure 4c,e,g.

A Luneburg spherical lens can focus any parallel radiation incident on a point on the surface to the opposite side of the sphere (and vice versa), as shown in Figure 4c, where an incident planewave with $\lambda = 300\,\mu m$ (≈1 THz) impinges on the sphere. No reflection occurs at the surface, as the refractive indexes at the surface and the surrounding medium are the same. This lens is obtained with a refractive index that varies as $n(r) = \sqrt{2 - (R/r)^2}$, where r is the radial coordinate and R is the sphere radius.

On the other hand, a Maxwell's fish-eye lens can guide light rays from one point source on a spherical surface, and focus them at the opposite point on the sphere, as shown in Figure 4e. In order to get such behavior, the refractive index has to change in the following way $n(r) = 2/(1 + (r/R)^2)$.

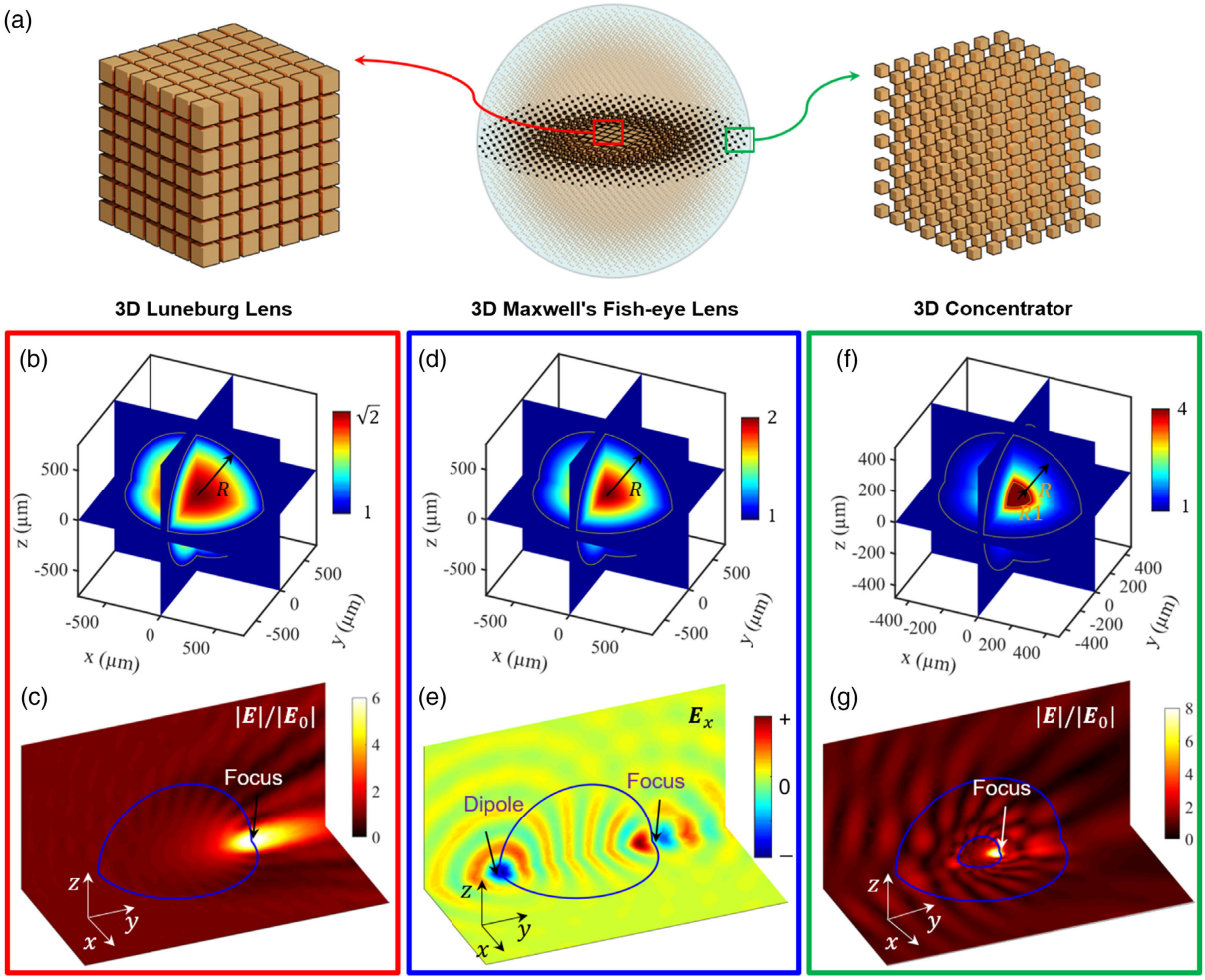

Figure 4. GRIN lenses. a) Schematics of a GRIN lens composed of metal nanoparticles with different sizes. Refractive index profiles for three GRIN lenses: b) Luneburg lens, $n(r) = \sqrt{2 - (r/R)^2}$; d) Maxwell's fish-eye lens, $n(r) = 2/(1 + (r/R)^2)$; f) light concentrator, $n(r) = R/r$. R is the radius of the each lens, r denotes the distance to the center, and $n(r)$ is the position-dependent refractive index. In (f) $R_1 = 100$ nm denotes the radius of the region with $n_{\text{eff}} = 4$. c) Amplitude of the electric field for the Luneburg lens. e) X-component of the electric field for the Maxwell's fish-eye lens. g) Amplitude of the electric field for the light concentrator. For all simulations, the incidence wavelength is $\lambda = 300\,\mu$m (≈1 THz). For (c) and (g), an x-polarized planewave is incident from the left side. The simulations are done using FEM.

In an ideal so-called "concentrator" lens, the focal point is located at the origin, and light impinging on the sphere will be focused on the center of the sphere. In this case the refractive index varies as $n(r) = R/r$ and at the origin needs to be infinitely high. In realistic systems, this limit cannot be attained, so we truncate the effective index of the lens at $n_{\text{eff}} = 4$ when $r = R_1 = R/3$ (Figure 4f), which produces sufficiently good quality of the focus, as shown in Figure 4g. We refer to these structures as *light sink* particles. Note that the electric field is strongly localized in the gaps between nanoparticles as a consequence of its discontinuity across the air–metal interfaces, producing intense, "doubly enhanced" electric field hotspots at the focal point.[16] Such structures can be extremely important in nonlinear optics.

Unlike plasmonic metamaterials in previous studies, the metaldielectrics proposed here are not based on lossy resonances and are both broadband and low loss. In addition to designing interesting devices using the concepts of transformation optics, metaldielectrics provide a promising optical material platform for numerous applications with versatile functionalities which demand composition materials with exotic optical properties.

2.3. Metasurfaces

Lenses are basic optical components, which have been widely used in various optical systems. Conventional optical lenses composed of transparent materials rely on cumulative effects on the waves passing through, and thus they are usually bulky and heavy. To solve this bottleneck, metasurface lenses have emerged as promising candidates of conventional lenses, using subwavelength antennas to interact with the wavefronts directly and tailor their shape and phase.[42] However, there are difficulties associated with metasurfaces—and among the most prominent are narrow-bandwidth and chromatic aberration. Those are because

many designs of the most efficient metasurfaces are based on resonators, which usually have sharp resonances. Otherwise, they have low efficiency. However, the material platform proposed here opens new opportunities in flat GRIN lenses designs, which are ultra-broadband and highly efficient. In **Figure 5**a,b, we show the schematic and refractive index profile of a flat GRIN lens, as a possible metasurface example, while Figure 5c shows its performance. We can appreciate that a thin metalens of just 300 μm, that is, just a wavelength thick in this case, can focus light as a classical bulky lens. The metalens in Figure 5a has a refractive index profile given by $n(r) = n_0 (1 - g^2 r^2/2)$ for $r < R$, where r denotes the distance to the center, g is a gradient parameter, n_0 is the maximum refractive index at the center, and R is the radius of the flat GRIN lens. In the calculation, we set $n_0 = 5$, $g = 562.183\,\mathrm{m}^{-1}$, and $R = 2250\,\mu\mathrm{m}$.

2.4. THz Adiabatic Focusing

Focusing light into subwavelength dimensions beyond the diffraction limit is notoriously difficult but is crucial in broad applications such as optical imaging. Some techniques including plasmonic nanofocusing have been proposed in the past[43] but these techniques possess some drawbacks. For example, plasmonic nanofocusing is based on plasmonic effects, which is usually narrowband and lossy. In addition, such designs are highly reliant on the optical properties of the materials available. The tapered waveguide schema in Figure 5d actually achieve focusing THz light into subwavelength dimensions, $\approx\lambda/10$, demonstrating the great advantages of light focusing using metaldielectrics. As case of study, the analysis was done at $\lambda = 300\,\mu\mathrm{m}$ ($\approx$1 THz) with an effective refractive index, $n = 4$, but such a device can work at any other frequency in the IR or lower energy. The near-field map in Figure 5e shows that the light is guided and focused at the taper apex with a diffraction-limited spot.

2.5. Artificial Birefringence

Birefringence is the optical property of anisotropic materials exhibiting different refractive indexes depending on the polarization and propagation direction of light. Birefringence has been used in many applications,[44,45] such as liquid-crystal displays and medical diagnostics. There are not many birefringent materials in nature, and a metamaterial approach is definitely welcome. Due to their symmetry in all directions, isotropic materials cannot be birefringent. However, mixtures composed of multiple isotropic materials can exhibit birefringence by tuning

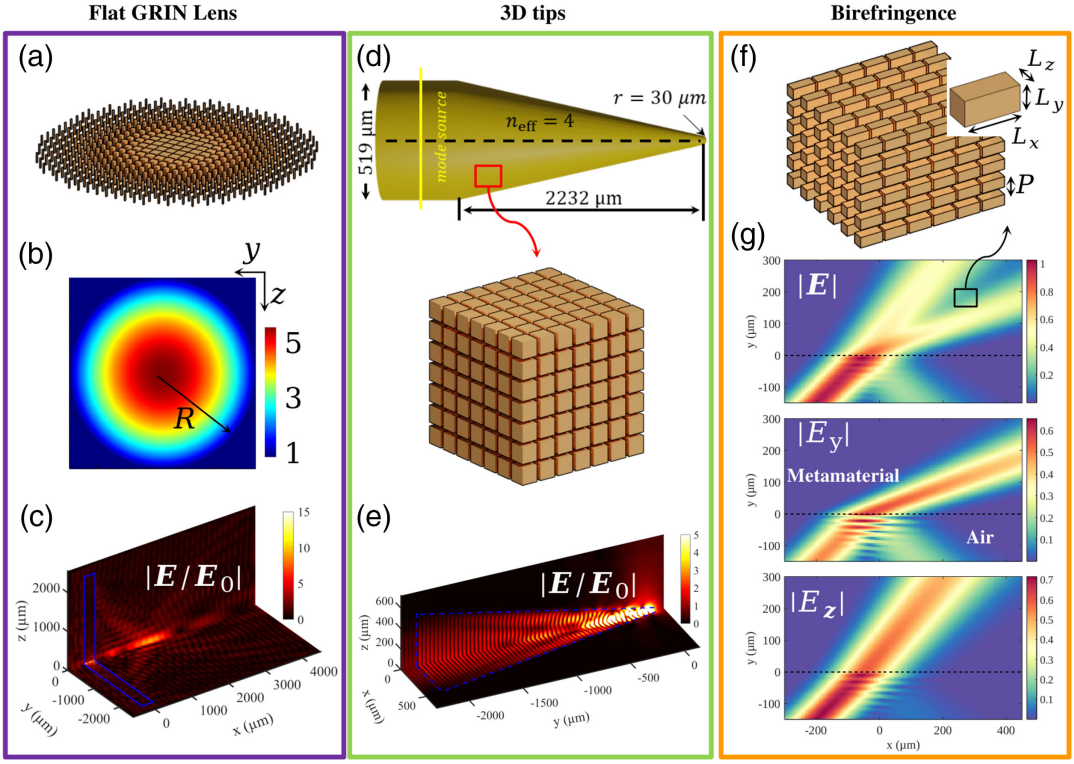

Figure 5. Focusing and birefringence. a) Schematic, b) refractive index profile, and c) amplitude of the electric field for a flat GRIN lens. The thickness of the lens is 300 μm. The source is a y-polarized planewave with wavelength of 300 μm, incident from the left side of the lens. d) Tapered waveguide and e) amplitude of the electric field when the source is the first fundamental mode generated by a mode source in Lumerical FDTD. The incident wavelength is 300 μm. f) Schematic of a birefringence metamaterial composed of gold cuboid nanocylinders (as shown in the inset) in a cubic lattice. g) Components of the electric field, when illuminated (from below) by an oblique planewave with wavelength of 30 μm using FDTD for the effective geometry in (f). The effective indexes were calculated based on the following parameters: $P = 50\,\mathrm{nm}$, $L_x = 46\,\mathrm{nm}$, $L_y = 10\,\mathrm{nm}$, and $L_z = 10\,\mathrm{nm}$. In the simulation, the diagonally anisotropic material has a permittivity of $[n_{xx}, n_{yy}, n_{zz}] = [3.4, 1.1, 1.1]$.

the "meta-atoms", as depicted in Figure 5f. In the simulation, we used gold cuboid nanocylinders with $L_x = 46\,\text{nm}$, and $L_y = L_z = 10\,\text{nm}$, and the period is set as $P = 50\,\text{nm}$ obtaining in this way $n_{\text{eff},x} \approx 3.4$ and $n_{\text{eff},y} = n_{\text{eff},z} \approx 1.1$. Figure 5g shows the components of the near field when a planewave impinges on a bulk metaldielectric composed of cuboid nanoparticles from the air side. Due to the asymmetry of the shape of the "meta-atoms", the metamaterial as a whole is birefrigent, although the constituent materials are isotropic.

3. Conclusion

In conclusion, we first introduced the concept of metaldielectrics by analogy with the natural dielectrics. We then extracted the effective parameters of the metaldielectrics using a numerical homogenization method[16] and demonstrated that the material platform proposed offers great advantages over conventional infrared materials, such as small dispersion and high transparency (low loss) over ultra-broadband ranges of wavelengths, enabling us to design broadband, high-transmission infrared and terahertz devices. More importantly, the local refractive indices can be tuned by structural geometry and the constituent materials in metaldielectrics, offering a promising solution for GRIN devices. The validation of the theory and the accuracy of the calculations were confirmed by comparing the results of the effective geometry and the full geometry simulations. Furthermore, we highlighted the inherently programmable properties of metaldielectrics by constructing a GRIN coating and GRIN lenses and demonstrated that such materials can be used in numerous applications with versatile functionalities, which demand composition materials with exotic optical properties.

Supporting Information

Supporting Information is available from the Wiley Online Library or from the author.

Acknowledgements

This work was supported by the Ministerio de Ciencia Innovacion/AEI and the European Union Next Generation/PRTR (PID2020-120306RB-I00 and PDC2021-121787-I00), the AGAUR (2017SGR883), the Universitat Rovira i Virgili (2021PFR-URV-B2-02), and the European Union's Horizon 2020 research and innovation programme under the Marie Skłodowska-Curie grant agreement no. 713679. V.G. acknowledges the Spanish Ministerio de Economia y Competitividad for financial support through the grant NANOTOPO (FIS2017-91413-EXP) and also the Ministerio de Ciencia, Innovación y Universidades through the grant MELODIA (PGC2018-095777-B-C21). The authors thank Dr. Daan M. Arroo, Samuel Palmer, and Ory Schnitzer for comments and suggestion on the manuscript. V.G. thanks the "ENSEMBLE3 - Centre of Excellence for nanophotonics, advanced materials and novel crystal growth-based technologies" project (GA no. MAB/2020/14), carried out within the International Research Agendas programme of the Foundation for Polish Science cofinanced by the European Union under the European Regional Development Fund and the European Union's Horizon 2020 research and innovation programme Teaming for Excellence (GA. no. 857543) for support of this work. S.A.M. acknowledges the ARC (DP220102152), the EPSRC (EP/W017075/1) and the Lee-Lucas Chair in Physics.

Conflict of Interest

The authors declare no conflict of interest.

Data Availability Statement

The data that support the findings of this study are available from the corresponding author upon reasonable request.

Keywords

metamaterials, nanoparticles, nanophotonics, THz photonics, transparent metals

Received: July 8, 2022
Published online: September 1, 2022

[1] J. B. Pendry, D. Schurig, D. R. Smith, *Science* **2006**, *312*, 1780.
[2] A. M. Urbas, Z. Jacob, L. Dal Negro, N. Engheta, A. Boardman, P. Egan, A. B. Khanikaev, V. Menon, M. Ferrera, N. Kinsey, C. DeVault, J. Kim, V. Shalaev, A. Boltasseva, J. Valentine, C. Pfeiffer, A. Grbic, E. Narimanov, L. Zhu, S. Fan, A. Alù, E. Poutrina, N. M. Litchinitser, M. A. Noginov, K. F. MacDonald, E. Plum, X. Liu, P. F. Nealey, C. R. Kagan, C. B. Murray, et al., *J. Opt.* **2016**, *18*, 093005.
[3] S. Lee, S. Baek, T. T. Kim, H. Cho, S. Lee, J. H. Kang, B. Min, *Adv. Mater.* **2020**, *32*, 2000250.
[4] J. A. Fan, C. Wu, K. Bao, J. Bao, R. Bardhan, N. J. Halas, V. N. Manoharan, P. Nordlander, G. Shvets, F. Capasso, *Science* **2010**, *328*, 1135.
[5] J. A. Fan, Y. He, K. Bao, C. Wu, J. Bao, N. B. Schade, V. N. Manoharan, G. Shvets, P. Nordlander, D. R. Liu, F. Capasso, *Nano Lett.* **2011**, *11*, 4859.
[6] J. A. Fan, K. Bao, L. Sun, J. Bao, V. N. Manoharan, P. Nordlander, F. Capasso, *Nano Lett.* **2012**, *12*, 5318.
[7] A. Poddubny, I. Iorsh, P. Belov, Y. Kivshar, *Nat. Photonics* **2013**, *7*, 948.
[8] V. M. Shalaev, *Nat. Photonics* **2007**, *1*, 41.
[9] S. A. Maier, *Plasmonics: Fundamentals and Applications*, Springer, New York **2007**.
[10] V. Giannini, A. Berrier, S. A. Maier, J. A. Sánchez-Gil, J. G. Rivas, *Opt. Express* **2010**, *18*, 2797.
[11] S. Bagavathiappan, B. Lahiri, T. Saravanan, J. Philip, T. Jayakumar, *Infrared Phys. Technol.* **2013**, *60*, 35.
[12] G. Hong, A. L. Antaris, H. Dai, *Nat. Biomed. Eng.* **2017**, *1*, 1.
[13] A. Y. Pawar, D. D. Sonawane, K. B. Erande, D. V. Derle, *Drug Invent. Today* **2013**, *5*, 157.
[14] W. T. Chen, A. Y. Zhu, V. Sanjeev, M. Khorasaninejad, Z. Shi, E. Lee, F. Capasso, *Nat. Nanotechnol.* **2018**, *13*, 220.
[15] J. Jung, H. Park, J. Park, T. Chang, J. Shin, *Nanophotonics* **2020**, *9*, 3165.
[16] S. J. Palmer, X. Xiao, N. Pazos-Perez, L. Guerrini, M. A. Correa-Duarte, S. A. Maier, R. V. Craster, R. A. Alvarez-Puebla, V. Giannini, *Nat. Commun.* **2019**, *10*, 1.
[17] J. H. Huh, J. Lee, S. Lee, *Nano Lett.* **2020**, *20*, 4768.
[18] S. Kim, C. Y. Zheng, G. C. Schatz, K. Aydin, K. H. Kim, C. A. Mirkin, *Nano Lett.* **2020**, *20*, 8096.
[19] W. Kock, *Bell Labs Tech. J.* **1948**, *27*, 58.
[20] S. Lee, *Opt. Express* **2015**, *23*, 28170.
[21] K. Chung, R. Kim, T. Chang, J. Shin, *Appl. Phys. Lett.* **2016**, *109*, 021114.

[22] D. Doyle, N. Charipar, C. Argyropoulos, S. A. Trammell, R. Nita, J. Naciri, A. Piqué, J. B. Herzog, J. Fontana, *ACS Photonics* **2017**, *5*, 1012.
[23] R. Kim, K. Chung, J. Y. Kim, Y. Nam, S. H. K. Park, J. Shin, *ACS Photonics* **2018**, *5*, 1188.
[24] J. H. Huh, K. Kim, E. Im, J. Lee, Y. Cho, S. Lee, *Adv. Mater.* **2020**, *32*, 2001806.
[25] A. Lauri, L. Velleman, X. Xiao, E. Cortes, J. B. Edel, V. Giannini, A. Rakovich, S. A. Maier, *ACS Photonics* **2017**, *4*, 2070.
[26] R. A. Alvarez-Puebla, E. R. Zubarev, N. A. Kotov, L. M. Liz-Marzán, *Nano Today* **2012**, *7*, 6.
[27] S. Gómez-Graña, J. Pérez-Juste, R. A. Alvarez-Puebla, A. Guerrero-Martnez, L. M. Liz-Marzán, *Adv. Opt. Mater.* **2013**, *1*, 477.
[28] L. Xu, H. Chen, *Nat. Photonics* **2015**, *9*, 15.
[29] B. Das, H. S. Yun, N. Park, J. Jeong, D. S. Kim, *Adv. Opt. Mater.* **2021**, *9*, 2002164.
[30] D. Kim, H. S. Yun, B. Das, J. Rhie, P. Vasa, Y. I. Kim, S.-H. Choa, N. Park, D. Lee, Y.-M. Bahk, D.-S. Kim, *Nano Lett.* **2021**, *21*, 4202.
[31] M. Tebbe, S. Lentz, L. Guerrini, A. Fery, R. A. Alvarez-Puebla, N. Pazos-Perez, *Nanoscale* **2016**, *8*, 12702.
[32] J. Gómez Rivas, G. Vecchi, V. Giannini, *New J. Phys.* **2008**, *10*, 105007.
[33] M. B. Ross, M. G. Blaber, G. C. Schatz, *Nat. Commun.* **2014**, *5*, 4090.
[34] A. Sihvola, *Photonics Nanostruct. Fundam. Appl.* **2013**, *11*, 364.
[35] V. A. Markel, *J. Opt. Soc. Am. A* **2016**, *33*, 1244.
[36] D. Smith, D. Vier, T. Koschny, C. Soukoulis, *Phys. Rev. E* **2005**, *71*, 036617.
[37] D. R. Smith, J. B. Pendry, *J. Opt. Soc. Am. B* **2006**, *23*, 391.
[38] A. D. Rakić, A. B. Djurišić, J. M. Elazar, M. L. Majewski, *Appl. Opt.* **1998**, *37*, 5271.
[39] M. Choi, S. H. Lee, Y. Kim, S. B. Kang, J. Shin, M. H. Kwak, K.-Y. Kang, Y.-H. Lee, N. Park, B. Min, *Nature* **2011**, *470*, 369.
[40] M. Born, E. Wolf, *Principles of Optics*, Cambridge University Press, Cambridge **1999**.
[41] N. Talebi, S. Meuret, S. Guo, M. Hentschel, A. Polman, H. Giessen, P. A. van Aken, *Nat. Commun.* **2019**, *10*, 1.
[42] D. Neshev, I. Aharonovich, *Light Sci. Appl.* **2018**, *7*, 1.
[43] D. K. Gramotnev, S. I. Bozhevolnyi, *Nat. Photonics* **2014**, *8*, 13.
[44] H. Mori, Y. Itoh, Y. Nishiura, T. Nakamura, Y. Shinagawa, *Jpn. J. Appl. Phys.* **1997**, *36*, 143.
[45] V. Ushenko, M. Gorsky, *Opt. Spectrosc.* **2013**, *115*, 290.